

Quantum error mitigation for fault-tolerant quantum computing

Yasunari Suzuki,^{1,2,*} Suguru Endo,^{1,†} Keisuke Fujii,^{3,4,5} and Yuuki Tokunaga^{1,‡}

¹*NTT Secure Platform Laboratories, NTT Corporation, Musashino 180-8585, Japan*

²*JST, PRESTO, 4-1-8 Honcho, Kawaguchi, Saitama, 332-0012, Japan*

³*Graduate School of Engineering Science, Osaka University,*

1-3 Machikaneyama, Toyonaka, Osaka 560-8531, Japan

⁴*Center for Quantum Information and Quantum Biology,*

Institute for Open and Transdisciplinary Research Initiatives, Osaka University, Japan

⁵*Center for Emergent Matter Science, RIKEN, Wako Saitama 351-0198, Japan*

Fault-tolerant quantum computing (FTQC) implements universal quantum computing while suppressing physical errors via quantum error correction. Although the effective error rate decreases exponentially with the code distance, it is expected that the number of available physical qubits is restricted even after FTQC is realized in some form. Meanwhile, quantum error mitigation (QEM) was recently introduced for suppressing errors in Noisy Intermediate-Scale Quantum (NISQ) devices for improving computation accuracy of near-term quantum algorithms with its overhead being a greater number of samples. In this work, we show QEM can compensate dominant errors in FTQC without increasing the number of qubits. This scheme will dramatically alleviate required overheads of FTQC for achieving a high-accuracy quantum computing.

I. INTRODUCTION

Quantum computers are believed to be capable of implementing several tasks such as factoring and Hamiltonian simulation with exponentially smaller computational time than classical computers [1, 2]. However, quantum systems generally interact with their environments, which leads to physical errors in the system and may destroy the quantum advantage. Since physical error rates of quantum computers are still much higher than those of classical computers, it is vital to suppress them.

There are two directions to overcome this problem. One is fault-tolerant quantum computing (FTQC) using quantum error-correcting codes [3–7]. We encode information of qubits to a logical code space constructed by several noisy physical qubits. It is shown that the effective error probability can be made arbitrarily small by increasing the number of physical qubits as long as error probabilities of physical qubits are smaller than a certain threshold determined by the code. Note that the overhead of FTQC is the number of qubits, which increases polynomially with the code distance, and the time for each quantum operation also scales linearly with the code distance accordingly.

The other direction is quantum error mitigation (QEM) [8–17]. Generally, QEM are used to mitigate physical errors in Noisy Intermediate-Scale Quantum (NISQ) devices and improve the computation accuracy of near-term quantum algorithms such as the variational quantum eigensolver. QEM relies on a post-processing of measurement outcomes and recover the expectation values of observables measured on quantum processors,

and hence does not require encoding of qubits. Instead, QEM necessitates a greater sample number as an overhead, which generally increases exponentially with the number of error events in the quantum circuit.

So far, huge efforts have been made for improving these two directions independently. For FTQC, one of the most promising approach is FTQC with lattice surgery [6, 7] with logical qubits encoded with surface codes [18, 19]. On the other hand, one of the most useful QEM method is probabilistic error cancellation because it can fully eliminate Markovian gate errors by inverting the noise process with recovery operations of QEM probabilistically applied in a quantum circuit, provided we can characterize physical errors in advance [8, 10].

Here, we propose and analyse an efficient framework for FTQC where QEC and QEM are combined on an equal footing. In this paper, we investigate how QEM should be adopted to an architecture of FTQC and show that a more accurate expectation value can be calculated with the same hardware requirement by QEM. Specifically, we show that probabilistic error cancellation, which is a technique of QEM, can mitigate two dominant errors in FTQC with a small overhead. They are decoding errors due to insufficient code distances and approximation errors induced by Solovay-Kitaev decomposition [20, 21], which we simply call decoding errors and approximation errors throughout this paper. We remark that there are crucial problems for performing probabilistic error cancellation for the two types of errors on the logical space, which we solved in an affirmative way. First, to apply probabilistic error cancellation, we need a good characterization of a noise model to compute recovery operations for a noise map. For this point, we show that decoding errors can be effectively considered as a stochastic Pauli map. Here, the noise map is evaluated either with process tomography or gate set tomography [22, 23] on the code space. Approximation errors by Solovay-Kitaev algorithm can be characterised efficiently on clas-

* yasunari.suzuki.gz@hco.ntt.co.jp

† suguru.endo@hco.ntt.co.jp; Y.S and S.E contributed to this work equally

‡ yuuki.tokunaga.bf@hco.ntt.co.jp

sical computers. Secondly, recovery operations of probabilistic error cancellation must be compatible with the architecture of FTQC. To cope with noisy syndrome measurements and restricted transversal operations, several techniques such as Pauli frame and magic state distillation are employed in FTQC. It is not trivial whether we can perform probabilistic error cancellation along with these techniques. We show that recovery operations of probabilistic error cancellation for these two types of errors can be properly constructed in FTQC. In this paper, we briefly review concepts of FTQC and QEM, and we show a low-overhead FTQC framework incorporating QEM. We evaluate an overhead of sampling cost for decoding and approximation errors and derive the necessary and sufficient conditions that should be satisfied for probabilistic error cancellation to be useful. Then, we numerically show our framework can actually reduce a code distance and the number of T -gates which are required for estimating expectation values within a given accuracy.

This paper is organized as follows. First, we illustrate probabilistic error cancellation in Sec. II. We review an architecture of fault-tolerant quantum computing in Sec. III. Then we describe how to evaluate decoding errors and approximation errors and have analytical argument of the cost of QEM in Sec. IV. Next, we also numerically analyze the cost of QEM for decoding errors and approximation errors, and we can effectively increase a code distance and the number of T -gates via QEM in Sec. V. Finally, we conclude our paper with discussions in Sec. VI.

II. QUANTUM ERROR MITIGATION AND PROBABILISTIC ERROR CANCELLATION

There generally exist physical noises in quantum processors, which should be mitigated to obtain correct results. For simplicity, here we assume gate errors are Markovian, i.e., a noise process \mathcal{N} for a gate is totally independent of other gate errors. In this case, we have

$$\rho_{\text{out}} = \mathcal{N}_{N_G} \circ \mathcal{U}_{N_G} \circ \mathcal{N}_{N_G-1} \circ \mathcal{U}_{N_G-1} \cdots \mathcal{N}_1 \circ \mathcal{U}_1(\rho_{\text{in}}), \quad (1)$$

where ρ_{out} and ρ_{in} are the output and input quantum states, \mathcal{U}_k and \mathcal{N}_k denote the ideal and noisy part of the process of the k -th gates, and N_G is the number of gates. To have the correct computation results, it is necessary to mitigate the effect of \mathcal{N}_k , ($k = 1, 2, \dots, N_G$) to obtain

$$\rho_{\text{out}}^{\text{ideal}} = \mathcal{U}_{N_G} \circ \mathcal{U}_{N_G-1} \cdots \circ \mathcal{U}_1(\rho_{\text{in}}). \quad (2)$$

Quantum error mitigation (QEM) is proposed as a method for suppressing errors without encoding, which is useful especially for NISQ devices with a restricted number of qubits [8–10]. Generally, QEM methods recover not the ideal density matrix $\rho_{\text{out}}^{\text{ideal}}$ itself, but the ideal expectation value of an observable $\langle \hat{M} \rangle_{\text{ideal}} = \text{Tr}(\rho_{\text{out}}^{\text{ideal}} \hat{M})$

via classical post-processing. Note that QEM is not a scalable technique because the cost for QEM needs exponentially increasing circuit runs with the number of error events in the quantum circuit [8, 10].

Now we explain probabilistic error cancellation with which we can eliminate a bias of an expectation value of observables completely given the complete information of the noise model [8, 10]. We will apply this method to suppress errors in FTQC later.

First, we identify the noise map \mathcal{N} via either process or gate set tomography [22, 23], and calculate the inverse \mathcal{N}^{-1} . Then, by finding a set of processes $\{\mathcal{B}_i\}$ such that $\mathcal{N}^{-1} = \sum_i \eta_i \mathcal{B}_i$ where $\eta_i \in \mathbb{R}$ and $\sum_i \eta_i = 1$, we have

$$\begin{aligned} \mathcal{U} &= \mathcal{N}^{-1} \mathcal{N} \mathcal{U} \\ &= \sum_i \eta_i \mathcal{B}_i \mathcal{N} \mathcal{U}. \end{aligned} \quad (3)$$

We remark that the linear combination of Clifford operations and measurement and tensor products of them can represent arbitrary operations [10]. We can rewrite Eq. (3)

$$\mathcal{U} = \gamma_Q \sum_i q_i \text{sgn}(\eta_i) \mathcal{B}_i \mathcal{N} \mathcal{U}, \quad (4)$$

where $\gamma_Q = \sum_i |\eta_i|$, $q_i = \frac{|\eta_i|}{\gamma_Q}$, $\gamma_Q \geq 1$ and $\text{sgn}(\eta_i)$ is a parity which takes ± 1 , corresponding to the operation \mathcal{B}_i . We refer to as γ_Q as QEM cost because it is related to sampling overhead.

Now suppose we measure an observable \hat{M} and obtain

$$\langle \hat{M} \rangle_{\mathcal{U}} = \gamma_Q \sum_i q_i \langle \hat{\mu}_i^{\text{eff}} \rangle. \quad (5)$$

Here, $\hat{\mu}_i^{\text{eff}} = \text{sgn}(\eta_i) \hat{m}^{(i)}$, and \hat{m}_i is a measurement outcome for a process $\mathcal{B}_i \mathcal{N} \mathcal{U}$. We generate the process \mathcal{B}_i with a probability q_i and multiply the corresponding parity to the measurement result, which is denoted as $\hat{\mu}_i^{\text{eff}}$. Then the expectation value of the random variable $\hat{\mu}^{\text{mit}} = \gamma_Q \hat{\mu}^{\text{eff}}$ approximates the error-free expectation value $\langle \hat{M} \rangle_{\mathcal{U}}$. Note that since $\text{Var}[\hat{\mu}^{\text{mit}}] = \gamma_Q^2 \text{Var}[\hat{\mu}^{\text{eff}}]$ and a measurement outcome without QEM which we denote $\hat{\mu}^{\text{mit}}$ has a similar variance, the variance of error-mitigated value is approximately amplified with $\Gamma_Q = \gamma_Q^2$. Therefore we need to have Γ_Q times more samples to achieve a similar accuracy before applying QEM.

In practice, probabilistic error cancellation is employed in a quantum circuit. The ideal process of the entire quantum circuit is described as $\prod_{k=1}^{N_G} \mathcal{U}_k$. Denoting $\mathcal{U}_k = \gamma_Q^{(k)} \sum_{i_k} q_{i_k} \text{sgn}(\eta_{i_k}) \mathcal{B}_{i_k} \mathcal{N}_k \mathcal{U}_k$, we have

$$\prod_{k=1}^{N_G} \mathcal{U}_k = \prod_{k=1}^{N_G} \gamma_Q^{(k)} \sum_{i_1 i_2 \dots i_{N_G}} \prod_{k=1}^{N_G} q_{i_k} \prod_{k=1}^{N_G} \text{sgn}(\eta_{i_k}) \prod_{k=1}^{N_G} \mathcal{B}_{i_k} \mathcal{N}_k \mathcal{U}_k. \quad (6)$$

From Eq. (6), we can see that in each gate we generate a process \mathcal{M}_{i_k} with probability q_{i_k} , and multiply

the product of parities $\prod_{k=1}^{N_g} \text{sgn}(\eta_{i_k})$ to the measurement results to obtain the outcome $\hat{\mu}^{\text{eff}}$. This procedure is repeated, and the product of the mean of outcomes $\langle \hat{\mu}^{\text{eff}} \rangle$ and $\gamma_Q^{\text{tot}} = \prod_{k=1}^{N_g} \gamma_Q^{(k)}$ approximates the correct expectation value. Note that now γ_Q^{tot} is the QEM cost for the entire quantum circuit. Let us assume the cost for each gate is uniform and can be approximated as $\gamma_Q^{(k)} = \gamma_Q = 1 + a\varepsilon$ with a and ε being a positive constant value and an effective error rate, respectively. Now the QEM cost and the sampling overhead can be approximated as $\gamma_Q^{\text{tot}} \simeq e^{a\varepsilon N_G} = e^{(\gamma_Q - 1)N_G}$ and $\Gamma_Q^{\text{tot}} = (\gamma_Q^{\text{tot}})^2$, which increase exponentially with the mean number of error events in the quantum circuit εN_G . Note that for $\varepsilon N_G = O(1)$ and $\varepsilon \rightarrow 0$, since $\varepsilon^k N_G = 0$ ($k \geq 2$), the QEM cost can be exactly described as $\gamma_Q^{\text{tot}} = e^{(\gamma_Q - 1)N_G}$.

III. FAULT-TOLERANT QUANTUM COMPUTING

A. Stabilizer formalism

In a framework of fault-tolerant quantum computing (FTQC), we prepare a redundant number of physical qubits and perform quantum computing in a code space defined as a subspace of the whole Hilbert space. By repetitively performing quantum error detection and correction, we can protect logical qubits defined in a code space against physical errors. A state of logical qubits is manipulated in a fault-tolerant manner with a set of logical operations.

Stabilizer formalism [3, 24] is the most standard way to construct quantum error-correcting codes. When we construct k logical qubits with n physical qubits, a 2^k -dimension code space \mathcal{C} is specified with a subgroup of n -qubit Pauli operators called stabilizer group. Let n -qubit Pauli group be

$$\mathcal{G}_n = \{\pm 1, \pm i\} \times \{I, X, Y, Z\}^{\otimes n}, \quad (7)$$

where I is an identity operator and $X = \begin{pmatrix} 0 & 1 \\ 1 & 0 \end{pmatrix}$, $Y = \begin{pmatrix} 0 & -i \\ i & 0 \end{pmatrix}$, $Z = \begin{pmatrix} 1 & 0 \\ 0 & -1 \end{pmatrix}$ are Pauli operators. A set of Pauli operator $\mathcal{S} \subset \mathcal{G}_n$ is called stabilizer group if \mathcal{S} is a commutative subgroup, the number of elements in \mathcal{S} is 2^{n-k} , and $-I \notin \mathcal{S}$. We denote a $(n-k)$ generator set of stabilizer group as $\mathcal{G} = (g_1, \dots, g_{n-k})$. The code space \mathcal{C} is defined as an eigenspace with $+1$ eigenvalues of all the operators in a stabilizer group, i.e., $\mathcal{C} = \{|\psi\rangle \mid \forall s_i \in \mathcal{S}, s_i |\psi\rangle = |\psi\rangle\}$. In the code space, we can introduce logical basis as $\{|0\rangle_L, |1\rangle_L\}^{\otimes k}$ and logical Pauli operators as $\{I_L, X_L, Y_L, Z_L\}^{\otimes k}$. A code distance d is defined as the minimum number of physical qubits on which an arbitrary logical operator except logical identity $I_L^{\otimes k}$ acts.

During quantum computation, physical errors which occurs on the encoded state are detected by measuring

$(n-k)$ Pauli operators, which is called stabilizer measurements, and the original state is restored by applying appropriate feedback operations estimated from obtained binary outcomes so-called syndrome values with a high success probability. The state is projected by a projector $P_s = \frac{1}{2}(I + (-1)^s g_i)$ with the i -th stabilizer measurement where $s \in \{0, 1\}$ is a syndrome value. During computation, we perform all the stabilizer measurements repetitively. One repetition of the stabilizer measurements is called a cycle of fault-tolerant quantum computing. If an effective error probability per physical qubit during a cycle is smaller than a certain threshold, we can estimate a Pauli operator which restores the original state with an exponentially small failure probability with the code distance d . Since the required number of physical qubit n increases polynomially to the code distance d in typical quantum error-correcting codes, we can exponentially decrease the logical error probability with polynomial qubit overhead.

B. Logical operations

We need to not only correct physical errors but also update a logical quantum state for computation. To this end, a universal set of logical operations should be done in a fault-tolerant manner. According to Solovay-Kitaev theorem [20, 21], we can approximate an arbitrary one- and two-qubit gates with a finite set of local operations.

For example, a set of Hadamard gate $H = \frac{1}{\sqrt{2}} \begin{pmatrix} 1 & 1 \\ 1 & -1 \end{pmatrix}$, controlled-not (CNOT) gate $\Lambda = |0\rangle\langle 0| \otimes I + |1\rangle\langle 1| \otimes X$, and T -gate $T = \exp(i\frac{\pi}{8}Z)$ is a universal gate set. Several logical operations can be done by transversally operating the same one- or two-qubit operations on physical qubits. Since transversal operations increase an effective physical error rate per qubit during a cycle constantly, we can fault-tolerantly achieve transversal logical operations. However, it is known that there is no stabilizer code of which the set of transversal gates is universal [25]. Thus, we need an additional technique to achieve fault-tolerant and universal quantum computing. The most promising solution is to create a quantum state called magic state and achieving non-transversal logical operations with gate teleportation [5]. Typically, we prepare a single-qubit logical state $|A\rangle = TH|0\rangle = \frac{1}{\sqrt{2}}(e^{i\pi/8}|0\rangle_L + e^{-i\pi/8}|1\rangle_L)$ as a magic state and perform T -gate by consuming a state $|A\rangle$. This magic state encoded in a logical qubit can be constructed with a process called magic state injection. While the infidelity of a magic state created by magic state injection is generally larger than a logical error rate, we can utilize magic state distillation to create a high-fidelity magic state from several noisy magic states only with transversal logical operations and logical measurements. Since the application of T -gates requires a longer time than the other operations, the number of T -gates is one of the most dominant factors of the whole computation time of FTQC.

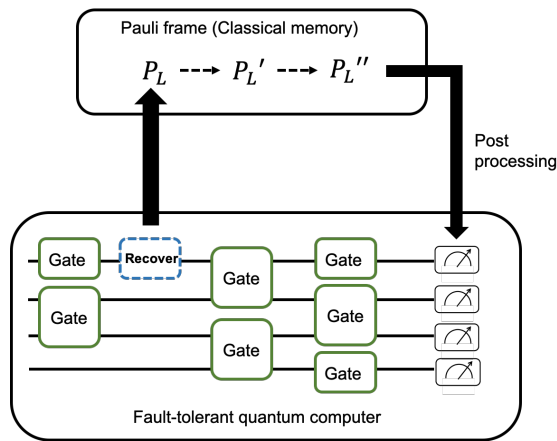


FIG. 1. Schematic figure of Pauli frame. The recovery operations are not physically applied on quantum computers but are stored on Pauli frame and efficiently updated after each Clifford gate operation. Depending on the state of Pauli frame, measurement outcomes are flipped.

Although we can estimate a Pauli operation for recovery from syndrome values, we do not apply it directly immediately after estimation. Instead, we store what Pauli operations should be applied to physical qubits for recovery in a classical memory called Pauli frame [5, 26], and it will be taken into account when we perform logical measurements and flip the outcome of logical measurements if required. The schematic figure is shown in Fig. 1. In the above construction of logical operations, the whole process except magic state injection consists only of Clifford operations and Pauli channels in a code space. Since a Pauli operator conjugated by a Clifford operator is also a Pauli operator, we can always track a recovery operator as a Pauli operator during computation. In addition, when we apply a logical Pauli operator to a state, we can perform it only by updating a Pauli frame since a logical Pauli operator is a transversal physical Pauli operator. As far as classical computers are reliable, this operation is effectively noiseless. Note that when we perform a destructive logical Pauli measurement, e.g., for T -gate teleportation, the measurement outcome is flipped due to the state of the Pauli frame and corresponding operations change accordingly.

IV. QUANTUM ERROR MITIGATION FOR FAULT-TOLERANT QUANTUM COMPUTING

In this section, we discuss how to apply QEM to FTQC. Here we consider two types of errors in FTQC: decoding errors due to failure of error estimation and approximation errors in Solovay-Kitaev decomposition. We discuss how these errors can be canceled with QEM and costs of QEM are evaluated.

A. Errors in fault-tolerant quantum computing

1. Decoding error

Here we describe a noise model in the logical space. In the absence of errors of ancillary qubits for syndrome measurements, we can perform recovery operations from syndrome values for each cycle independently. Thus, quantum states are in the logical code space when we perform estimated recovery operation regardless of whether estimation is correct or not. Note that recovery operations are not instantly applied in practice since they are Pauli operators and can be stored in the Pauli frame. In this case, we can define a noise map of a logical operator as \mathcal{M}_{dec} , which maps a logical state to another logical state. This map can be characterized by process or gate set tomography in advance.

However, in practice, noise may occur on ancillary qubits for syndrome measurements and thus outcomes of syndrome measurements may be flipped even when there are no errors on data qubits. When syndrome measurements are faulty, recovery operations are estimated after several cycles. This is because estimation of recovery operations for a certain cycle requires syndrome values in subsequent cycles and there is a latency in post-processing. Nevertheless, here we assume that we can define an effective logical error map for each logical operation and also assume that this noise map is a stochastic Pauli map. See Appendix. A for the justification of these assumptions. Then, we can describe a noise map for each logical operation \mathcal{N}_{dec} as the following non-uniform depolarizing channel:

$$\mathcal{N}_{\text{dec}}(\rho) = \sum_{g \in \{I_L, X_L, Y_L, Z_L\}} p_g g \rho g^\dagger, \quad (8)$$

where $p_g \in \mathbb{R}$, $\sum_g p_g = 1$ and $p_g \geq 0$. The sum of probabilities of non-identity logical operation is called a logical error probability p_{dec} , i.e., $p_{\text{dec}} = \sum_{g \neq I^{\otimes m}} p_g$. It is known that when physical error rate is sufficiently small, an effective logical error probability per syndrome-measurement cycle p_{cyc} decreases exponentially to a code distance d as

$$p_{\text{cyc}} \simeq C_1 \left(C_2 \frac{p}{p_{\text{th}}} \right)^{(d+1)/2}, \quad (9)$$

where p is a physical error rate, p_{th} is a threshold value, and C_1, C_2 are constants [27]. While constant values depend on details of error correction schemes, $C_1 \simeq 0.13$ and $C_2 \simeq 0.61$ are expected in the typical construction of surface codes and noise model [27, 28]. Thus, when a logical error probability is sufficiently small, we can approximate the logical error probability for d cycle p_{dec} as $p_{\text{dec}} = 1 - (1 - p_{\text{cyc}})^d \simeq d p_{\text{cyc}}$. Since the number of cycles per logical gate increases linearly with code distance d , this is considered as a logical error probability per logical gate. In practice, p_g for $g \neq I^{\otimes m}$ is exponentially small and is hard to evaluate by sampling in practice, $\{p_g\}$ can

be estimated by performing process tomography or gate-set tomography in logical space with small code distance d and extrapolating the result with Eq. (9). Note that while failure probability is generally dependent on logical operations, we assume it changes the threshold value p_{th} up to a constant factor.

2. Approximation errors

Since we are only allowed to use a limited set of logical operations for achieving fault-tolerance, we need to decompose an arbitrary unitary gate to a sequence of available gates. Any unitary operator can be decomposed into a product of CNOT gates and single-qubit gates. Thus, we need to approximate single-qubit gates with a given gate set to a desired accuracy. With an improved Solovay-Kitaev algorithm [29], given a universal gate set such as $\{T, H, S\}$, single-qubit gate U , we can construct an approximated gate \tilde{U} which satisfies $\varepsilon = \|\tilde{U} - U\|$ to an arbitrary accuracy ε as a sequence of given gate set with length $\tilde{O}(\log(\varepsilon^{-1}))$ with $\|\cdot\|$ being an operator norm. The error of approximated map is given by

$$\mathcal{N}_{SK}(\rho) = \tilde{U}U^\dagger \rho U\tilde{U}^\dagger. \quad (10)$$

Since this decomposition involves only single-qubit operations, this error channel can be evaluated in advance efficiently.

B. Quantum error mitigation for fault-tolerant quantum computing

Here, we discuss that decoding errors and approximation errors can be mitigated with probabilistic error cancellation.

1. Quantum error mitigation for decoding errors

We can express the inverse channel of the non-uniform depolarizing channel Eq. (8) as a linear combination of Pauli operations. Thus, we can express the inverse channel as

$$\begin{aligned} \mathcal{N}_{dec}^{-1}(\rho) &= \sum_{g \in \{I_L, X_L, Y_L, Z_L\}^{\otimes m}} \eta_g g \rho g^\dagger \\ &= \gamma_{dec} \sum_{g \in \{I_L, X_L, Y_L, Z_L\}^{\otimes m}} q_g \text{sgn}(\eta_g) g \rho g^\dagger. \end{aligned} \quad (11)$$

Refer to Appendix. C for concrete expression of each coefficient η_g , γ_{dec} , and q_g . Thus we can suppress the errors by applying probabilistic error cancellation only with Pauli operators after decoding processes. The QEM cost for decoding errors in the entire circuit can be expressed as $\gamma_{dec}^{\text{tot}} = \prod_{k=1}^{N_{dec}} \gamma_{dec}^{(k)}$, where N_{dec} is the number of logical gates, and $\gamma_{dec}^{(k)}$ is a QEM cost of the k -th operation.

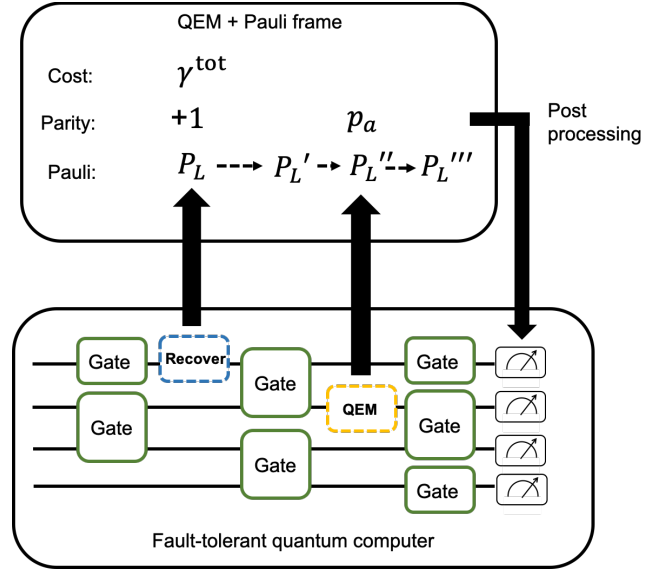


FIG. 2. Schematic figure for Pauli frame incorporating QEM. If a QEM recovery operation is a Pauli operation, it is not directly applied on the quantum computer but Pauli frame is updated instead. According to generated recovery operations of QEM, the parity is also updated. Here we denote the parity corresponding to the QEM recovery operation as p_a in the figure. If a QEM recovery operation is not a Pauli operator, it is physically performed. Then measurement outcomes are post-processed depending on the Pauli frame, parity, and QEM cost.

Note that probabilistic error cancellation usually applies recovery operations of QEM just after noisy gates [8, 10]; however, because we only operate logical Pauli operations for recovery operations on the logical space, they can be done only by updating Pauli frame instead of directly applying it after noisy gates. Finally, the measurement result is post-processed according to the state of the Pauli-frame, the parity corresponding to the applied recovery operations, and the QEM cost. The schematic figure is shown in Fig. 2. We remark that the information of the QEM cost and the parity is used only when the final measurement result is obtained; the outcome of a destructive logical Pauli measurement is flipped depending only on the state of the Pauli frame.

By approximating the QEM cost in the first order of the logical error, we can show

$$\gamma_{dec} \simeq 1 + 2p_{dec}. \quad (12)$$

Refer to Appendix. C for details. Under the assumption that the logical error rate is the same for all the logical operations and $p_{dec}N_{dec} = O(1)$ with $p_{dec} \rightarrow +0$, the QEM cost $\gamma_{dec}^{\text{tot}}$ for the entire quantum circuit is exactly equal to $e^{2p_{dec}N_{dec}}$ based on the argument in Sec. II. Thus, by using Eq. (9), we obtain

$$\gamma_{dec} - 1 = 2dC_1 \left(C_2 \frac{p}{p_{th}} \right)^{(d+1)/2}, \quad (13)$$

which results in the total QEM sampling overhead

$$\Gamma_L^{\text{tot}} = e^{2(\gamma_{\text{dec}}-1)N_{\text{dec}}} = \exp\left(4dC_1N_{\text{dec}}\left(C_2\frac{p}{p_{\text{th}}}\right)^{(d+1)/2}\right). \quad (14)$$

Notice that Eq. (14) clearly shows a trade-off relationship between the sampling overhead and the code distance, i.e., the number of physical qubits.

2. Quantum error mitigation for approximation errors

Unlike decoding errors due to failure of error correction, as Pauli twirling is not allowed for Solovay-Kitaev decomposition, we cannot convert approximation errors into stochastic Pauli errors. Nevertheless, we can still apply probabilistic error cancellation. Denote $\mathcal{N}_{\text{SK}}(\rho) = \tilde{U}U\rho(\tilde{U}U)^\dagger$, we invert this approximation error by

$$\begin{aligned} \mathcal{N}_{\text{SK}}^{-1} &= \sum_i \eta_i \mathcal{B}_i^{(L)} \\ &= \gamma_{\text{SK}} \sum_i q_i \text{sgn}(\eta_i) \mathcal{B}_i^{(L)}, \end{aligned} \quad (15)$$

where $\{\mathcal{B}_i^{(L)}\}$ is recovery operations on logical space. Note that we can represent any map as a linear combination of Clifford operations and Pauli channels [10], and thus we do not need T -gates for mitigating approximation errors. Recovery operations are randomly chosen and applied just after each single-qubit logical operation if they are not Pauli operations. In the case of Pauli operations, we can again use Pauli frame, and physical operations on quantum computers are not required in a similar vein to QEM for decoding errors. In numerical simulations in the next section, we will verify that

$$\gamma_{\text{SK}} - 1 = \beta_1 e^{-\beta_2 N_T}, \quad (16)$$

where β_1 and β_2 are constants dependent on a quantum gate and N_T is the number of available T -gates.

The QEM cost due to approximation errors can also be represented as $\gamma_{\text{SK}}^{\text{tot}} = \prod_{k=1}^{N_{\text{SK}}} \gamma_{\text{SK}}^{(k)}$, where N_{SK} is the total number of recovery operations for mitigating approximation errors in the quantum circuit with the cost $\gamma_{\text{SK}}^{(k)}$ corresponding to the k -th recovery operation. By assuming that the cost does not depend on gates, we have the following QEM sampling overhead:

$$\Gamma_{\text{SK}}^{\text{tot}} \simeq \exp(2\beta_1 N_{\text{SK}} e^{-\beta_2 N_T}), \quad (17)$$

This indicates a trade-off relationship between the sampling overhead and the number of available T -gates.

3. Measure for performance of quantum error mitigation

Now we discuss in what situation QEM is beneficial. Let $\gamma_Q^{\text{tot}} = \gamma_{\text{dec}}^{\text{tot}} \gamma_{\text{SK}}^{\text{tot}}$ be the QEM cost in the entire quantum circuit. The standard deviation of the expectation

value of the observable without QEM can be described as $\Delta_N = \sqrt{\text{Var}[\hat{\mu}^{\text{nmit}}]}/\sqrt{N}$ with N being the sample number. Suppose an expectation value of FTQC without QEM has a bias ϵ_{bias} to the exact value due to noise. Then, to achieve an accuracy within a given allowed estimation error ϵ without QEM, we need to have $\epsilon_{\text{bias}} + \Delta_N < \epsilon$. In the case of $\epsilon_{\text{bias}} > \epsilon$, this inequality never holds and QEM is always required. In the case of $\epsilon_{\text{bias}} \leq \epsilon$, we can consider that an allowed estimation error with QEM effectively reduces to $\epsilon - \epsilon_{\text{bias}}$. Thus, if the increase of a required number of sampling to achieve a given accuracy due to the residual bias is greater than that by QEM costs, QEM is also beneficial in this case. More precisely, the number of samples N must satisfy $N > N^{\text{nmit}} \equiv \sqrt{\text{Var}[\hat{\mu}^{\text{nmit}}]}/(\epsilon - \epsilon_{\text{bias}})^2$ without QEM. On the other hand, when we use QEM, we need $\gamma_Q^{\text{tot}} \sqrt{\text{Var}[\hat{\mu}^{\text{eff}}]}/\sqrt{N} < \epsilon$, hence we have $N > N^{\text{mit}} \equiv (\gamma_Q^{\text{tot}})^2 \text{Var}[\hat{\mu}^{\text{eff}}]/\epsilon^2$. We focus on measurement of Pauli operators because they are generally measured on quantum computers. Since $\langle \hat{\mu}^{\text{eff}} \rangle \simeq 0$ for $\gamma^{\text{tot}} \gg 1$ we have $\text{Var}[\hat{\mu}^{\text{eff}}] \simeq 1$, and necessarily $\text{Var}[\hat{\mu}^{\text{nmit}}] \leq 1$. Then there is an advantage of QEM when $N^{\text{mit}} < N^{\text{nmit}}$, which is equivalent to

$$\gamma_Q^{\text{tot}} \leq \frac{1}{1 - \frac{\epsilon_{\text{bias}}}{\epsilon}}. \quad (18)$$

Thus, QEM is required when an allowed estimation error ϵ is smaller than or close to the bias ϵ_{bias} . Based on the above argument, even when FTQC can achieve high accuracy, QEM should be employed to further improve calculation accuracy depending on the value of ϵ .

V. NUMERICAL ANALYSIS

In this section, we numerically evaluate how error mitigation can suppress the required qubit overhead in FTQC. First, we numerically investigate the efficiency of QEM for each factor of errors introduced in Sec. IV. See Appendix D for detailed settings and definitions of numerical analysis.

A. Quantum error mitigation for decoding errors

1. Cost analysis

First, we evaluate the performance of QEM for decoding errors during logical operations, where we assume FTQC with surface codes and lattice surgery. For details about surface codes, see Appendix B. For simplicity, we assume single-qubit depolarizing noise model occurs on each data and measurement qubits at the beginning of each cycle, which corresponds to a phenomenological noise model [30, 31]. To determine a failure probability of decoding with faulty syndrome-measurement cycles, we assume perfect syndrome measurements at the 0-th and

d -th cycles. Then we check whether logical Pauli- X, Y, Z errors occurred during d cycles. Recovery operations are estimated from syndrome values with minimum-weight perfect matching algorithm [18, 32]. We evaluate logical error probabilities of Pauli- X, Y, Z and compute a QEM cost for d cycles according to Eq. (C5). Despite the assumption of perfect syndrome measurements of 0-th and d -th cycle, we expect that numerical results become asymptotically equivalent to those without the assumption when d is sufficiently large.

Logical error probabilities of Pauli- X, Y, Z of a single logical qubit for several code distances are calculated, and the sum of their probabilities are plotted according to physical error rates in Fig. 3(a). A logical error probability is exponentially reduced according to the code distance when physical error probability p is smaller than a threshold value. A behavior of logical error probabilities around a threshold value is plotted in Fig. 3(b), which is around $p_{\text{th}} = 0.044$.

We compute QEM costs for decoding errors γ_{dec} corresponding to d cycles and different code distances, and compared them with the first order approximation shown in Eq. (12). Numerical results are plotted in Fig. 3(c). In this figure, solid lines correspond to an approximation of QEM costs in Eq. (12). We see that QEM costs also decay exponentially depending on the code distances and show a threshold behavior like logical error probabilities. They coincide well when physical error rate is sufficiently small.

2. Performance analysis

We demonstrate the performance of QEM for decoding errors in large-scale quantum circuits with a 100-qubit logical random Clifford circuit with 100 layers. In each layer, randomly generated single-qubit Clifford gates are simultaneously applied and then 50 CNOT gates are applied to randomly paired two qubits. Owing to an efficient algorithm of stabilizer circuits [24, 33], we can simulate these protocols efficiently. As an observable, we choose a Pauli operator whose measurement outcome is always unity for the final state vector if there are no physical errors, i.e., the final state is a +1 eigenstate of the chosen observable. In numerical simulations, we assume a non-uniform single-qubit depolarizing logical error in the form of Eq. (8) for each layer. Logical error probabilities of depolarizing channels are determined according to the numerical results of the last section. In this simulation, we choose $p = 0.01$, and logical error probabilities are obtained with extrapolation. Logical error probabilities that we estimate are summarized in TABLE I. Without QEM, the final state converges to a highly mixed state due to physical errors. Thus, it is expected that expectation values decay to zero. By employing QEM, they are taken back to unity, sacrificing statistical accuracy and requiring a greater number of experiments accordingly.

Note that while a required number of cycles for Clif-

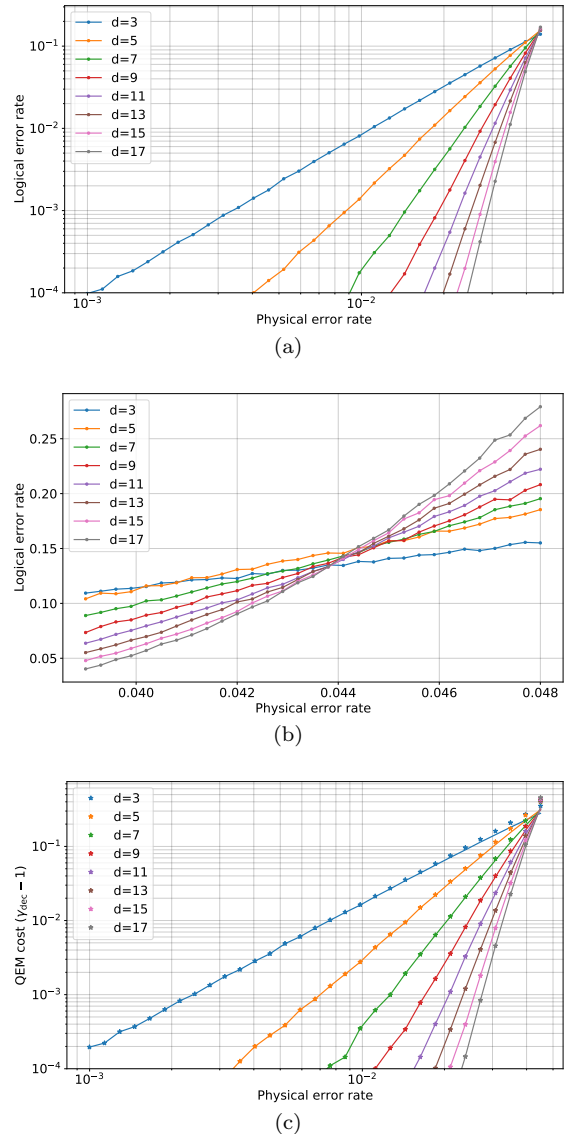


FIG. 3. Logical error probabilities and QEM costs for d -cycle syndrome measurements are plotted according to physical error rates at several code distances. (a) Logical error probabilities as a function of physical error rate. (b) The same figure zoomed around a threshold value. (c) QEM costs for d -cycle idling operations. The first order approximations from Eq. (12) are shown as solid lines.

ford operations scales linearly with the code distance, the actual number of cycles and logical error probability per logical gate are dependent on a Clifford operation. In particular, logical CNOT gates with lattice surgery may induce correlated logical Pauli errors on multiple logical qubits. Nevertheless, we use a simplified error model since we expect this evaluation captures basic properties of QEM performance.

We numerically perform a series of 10^4 experiments, each of which computes an expectation values with 10^4 single-shot measurements. The results are shown in

code distance d	p_{X_L}, p_{Z_L}	p_{Y_L}
5	1.80×10^{-4}	1.96×10^{-6}
7	1.39×10^{-5}	4.11×10^{-8}
9	1.08×10^{-6}	8.64×10^{-10}
11	8.35×10^{-8}	1.81×10^{-11}

TABLE I. Estimated logical error probabilities for code distances with $p = 0.01$ and $p_{\text{th}} \sim 0.044$.

Fig. 4(a), and detailed data around ideal expectation value is shown in Fig. 4(b). The mean value of 10^4 samples for each logical error probabilities are shown in Fig. 4(c) with its standard deviation as an error bar. We see there is a large bias in an expectation value without QEM. On the other hand, there is no bias when QEM technique is employed, while its standard deviation is amplified. A standard deviation of expectation values with $d = 5$ is 14.2, and thus not visible in the histogram because it is too large. The mean number of Pauli errors in the whole quantum circuit is 3.6 in $d = 5$ and 0.28 in $d = 7$. Thus, as explained in Sec. II, QEM is typically useful when the number of Pauli errors in the circuit is $O(1)$. Whether QEM is useful or not is dependent on a criterion shown in Sec. IV B 3. Thus, we see that QEM technique is effective in large-scale quantum computing, and enables us to increase effective code distance.

B. Quantum error mitigation for approximation errors

1. Cost analysis

Here, we study the performance of QEM under Solovay-Kitaev decomposition. Since the actual QEM cost γ_{SK} depends on a target unitary operator, we draw a sample of unitary operation U from Haar-measure random distribution μ_{H} . Then, we decompose a unitary gate in the form of $U = R_Z(\theta_1)\sqrt{X}R_Z(\theta_2)\sqrt{X}R_Z(\theta_3)$, where $\sqrt{X} = HSH$ is a Clifford operation. We use an improved Solovay-Kitaev algorithm shown in Ref. [29]. This algorithm enables us to approximate an arbitrary Pauli- Z rotation $R_Z(\theta) = \exp(i\frac{\theta}{2}Z)$ with an operator \tilde{U} which is described as a sequence of Clifford operations and T -gates. We set the maximum count of T -gate for each decomposition for three Pauli- Z rotations to check a trade-off relation between a T -gate count and an approximation accuracy. A histogram of errors evaluated with operator norm $\|U - \tilde{U}\|$ is shown in Fig. 5(a). As expected, an exponential decrease of approximation errors is observed.

Then, we calculate QEM costs by using Eq. (15). A histogram for QEM costs γ_{SK} is shown in Fig. 5(b). We show QEM costs versus the number of allowed T -gates in Fig. 5(c). We can see that $\gamma_{\text{SK}} - 1$ exponentially reduces according to the number of T -gates, and its variance also

decreases exponentially. We fit the QEM cost γ_{SK} with Eq. (16), and obtain $\beta_1 = 3.9(5)$ and $\beta_2 = 0.072(1)$.

2. Performance analysis

Next, we evaluate the performance of QEM for approximation errors due to Solovay-Kitaev decomposition via simulation of a SWAP test circuit with 7 qubits. A SWAP test circuit evaluates the overlap of two input states ρ and σ as $\text{Tr}[\rho\sigma]$ by measuring an ancilla qubits [34]. We set one of the input state to the ideal state and the other to the state affected by approximation errors. A schematic is shown in Fig. 6.

The ideal state is generated by random quantum circuits which consist of three layers. In each layer, random single-qubit unitary operations are simultaneously applied, then a CNOT gate acts on randomly chosen two qubits. The same random quantum circuit is applied to the approximated state by employing Solovay-Kitaev decomposition to each single-qubit rotation. If there are no approximation errors, since the input states are the same, we necessarily obtain +1 as measurement outcomes hence the expectation value is also +1 for the Pauli- Z operator of the ancilla qubit. On the other hand, an expectation value becomes smaller than unity when the inner product is reduced due to approximation errors. Since approximation errors cannot be treated in a framework of stabilizer simulation, we simulate quantum circuits by directly updating the state vector after each gate.

We also numerically perform a series of 10^4 experiments and compute expectation values from 10^4 single-shot measurements. The number of allowed T -gates in each Solovay-Kitaev decomposition for single-qubit unitary operations is chosen from 24 to 60. The results are shown in Fig. 4(a), and detailed data around ideal expectation value is shown in Fig. 4(b). The mean value of 10^4 samples for each logical error probabilities are shown in Fig. 4(c) with its standard deviation as an error bar. Note that standard deviation with 21 T -gates is 4.65. We see that our QEM technique successfully removes a bias of the expectation value in noisy cases. Compared to the QEM costs for decoding errors, we obtain larger QEM costs. This is consistent with the results reported in Ref. [10] that QEM costs for unitary errors tend to be larger than stochastic errors.

This problem may be relaxed by performing several Solovay-Kitaev decomposition with the same accuracy, constructing randomizing approximation errors, and removing coherent component of noise. Note that with a sufficiently large sample size, our QEM technique increases an effective number of T -gates by inserting additional Clifford gates and Pauli channels and repetitive sampling, which can be achieved with negligible additional hardware requirements.

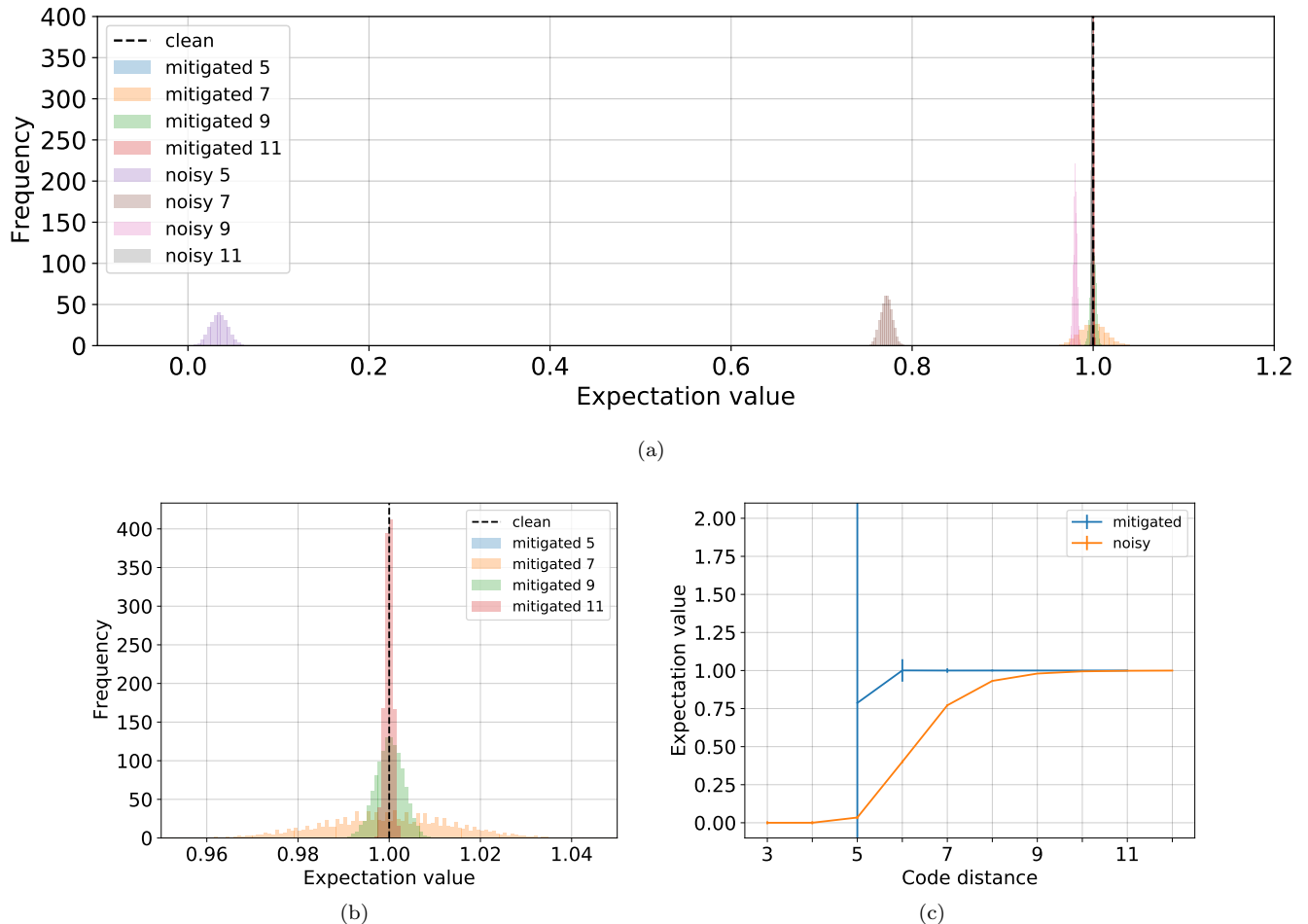


FIG. 4. (a) A histogram for expectation values for 100-qubit random Clifford circuits. (b) A histogram for expectation values with QEM for 100-qubit random Clifford circuits. (c) Sample averages and standard deviation of 100-qubit random Clifford circuits are plotted as a function of code distances.

VI. DISCUSSION

In this work, we show an approach to effectively decrease errors in FTQC by performing QEM in the logical space. In the case of decoding errors, owing to Pauli frame, we can perform QEM without implementing any physical operations if decoding errors are stochastic Pauli maps, while QEM induces additional errors when we implement it physically on general quantum circuits. For approximation errors by Solovay-Kitaev decomposition, we cannot always use Pauli frame because not only Pauli operations but also Clifford operations and Pauli measurements are employed for QEM in general. Since Clifford operations can be efficiently performed in FTQC and the number of decoding processes for error correction is much larger than the gate count in Solovay-Kitaev algorithms, this overhead is negligible. We also verify its trade-off between costs of QEM and the code distance and the number of T -gates. We show that our approach is always useful when an allowed estimation error is close to or smaller than the bias of the computation result with-

out QEM. Furthermore, we demonstrate our approach enables quantum computing corresponding to more than the achievable code distance and number of T -gates.

One of the promising application of our method is Hamiltonian simulation of quantum many-body dynamics. There are algorithmic errors in Trotter decomposition [35] and in recently proposed methods such as Taylor series [36] and quantum signal processing [37, 38]. As these errors involve the entire quantum computer, it is hard to estimate the probabilistic cancellation map. In Refs. [39, 40], it is shown that such algorithmic errors can be mitigated by employing extrapolation. Since algorithmic errors can be controlled by changing simulation accuracy, this technique can also be naturally applied in a FTQC scenario. Thus dominant errors in FTQC can be compensated via QEM.

The first generation of FTQC may not be sufficiently large for naively solving large and useful problems. While an architecture of distributed quantum computing is the most straight-forward approach to increase the total number of qubits, it requires interconnections between

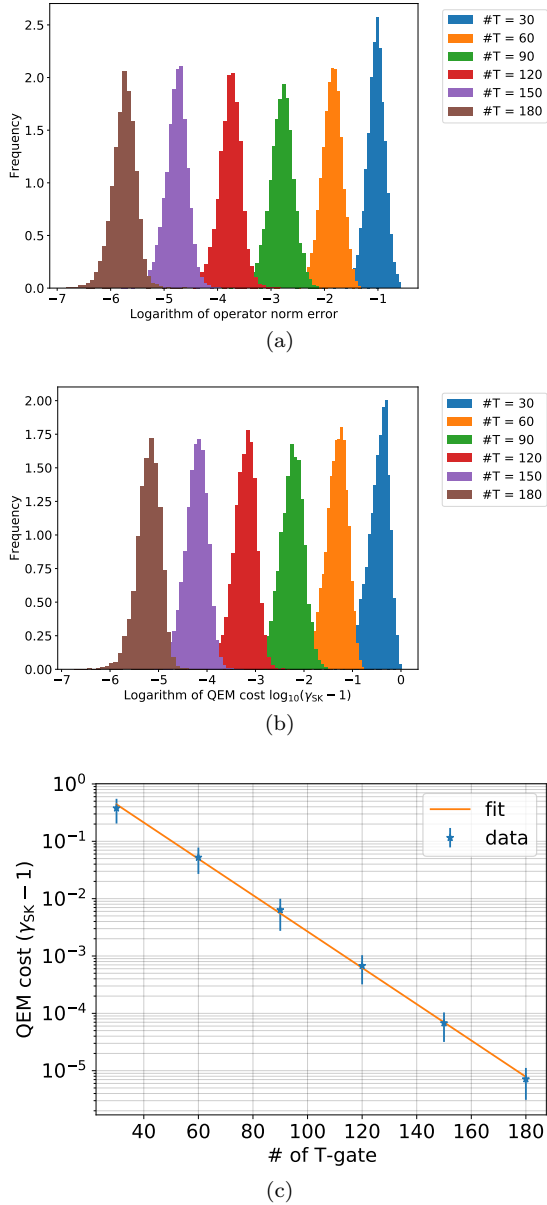


FIG. 5. Approximation errors and QEM costs of improved Solovay-Kitaev method are calculated for Haar-random unitary operations. Each color corresponds to the maximum count of T -gate. (a) A histogram of approximation errors due to Solovay-Kitaev decomposition. (b) A histogram for QEM costs. (c) A histogram of QEM costs for approximation errors as a function of the number of allowed T -gates.

quantum nodes, which induces additional overheads for entanglement distillation. Thus, we sometimes cannot use sufficient code distances for creating logical qubits. In this context, techniques developed in NISQ era [41, 42] for solving larger problems with small NISQ computers may also be useful in the middle-term FTQC. Our work is the first proposal that makes the best of a technique tailored for NISQ devices in a context of FTQC.

Finally, we discuss the difference between our scheme

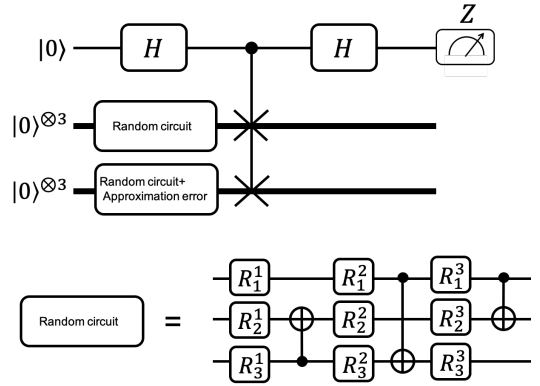


FIG. 6. Schematic figure for a 7-qubit SWAP test circuit we simulate. We calculate the overlap of randomly generated states and the approximation of the generated state via Solovay-Kitaev algorithm. The random circuit is constructed by three layers, each of which composes of random single-qubit rotation gates and CNOT gates to randomly chosen two qubits.

and a similar work which combines QEM with quantum error correction proposed by McClean *et al.* [43]. Their method considers implementing quantum error correction for NISQ devices via classical post-processing in the case that experimentalists cannot implement stabilizer measurements due to limited connectivity and large error rates of NISQ devices. Although their method enables projection of the state to the code space via quantum subspace expansion [44], logical errors cannot be fully eliminated. On the other hand, our scheme assumes FTQC can be performed but the number of qubits and T gates cannot be increased infinitely. The remarkable advantage of our method is that we can fully eliminate the decoding errors and approximation errors with a greater number of measurements with negligible hardware overhead, given the complete characterization of the noise model.

ACKNOWLEDGEMENT

This work is supported by PRESTO, JST, Grant No. JPMJPR1916; ERATO, JST, Grant No. JPMJER1601; CREST, JST, Grant No. JPMJCR1771; MEXT Q-LEAP Grant No. JPMXS0120319794 and JPMXS0118068682. S.E acknowledges useful discussions with Zhenyu Cai and Xiao Yuan.

Appendix A: Noise model in evaluation of decoding errors

Here, we explain how our assumptions on a noise model of decoding errors as Eq. (8) are justified in FTQC with faulty syndrome measurements. When syndrome measurement may output a wrong value, we need successive

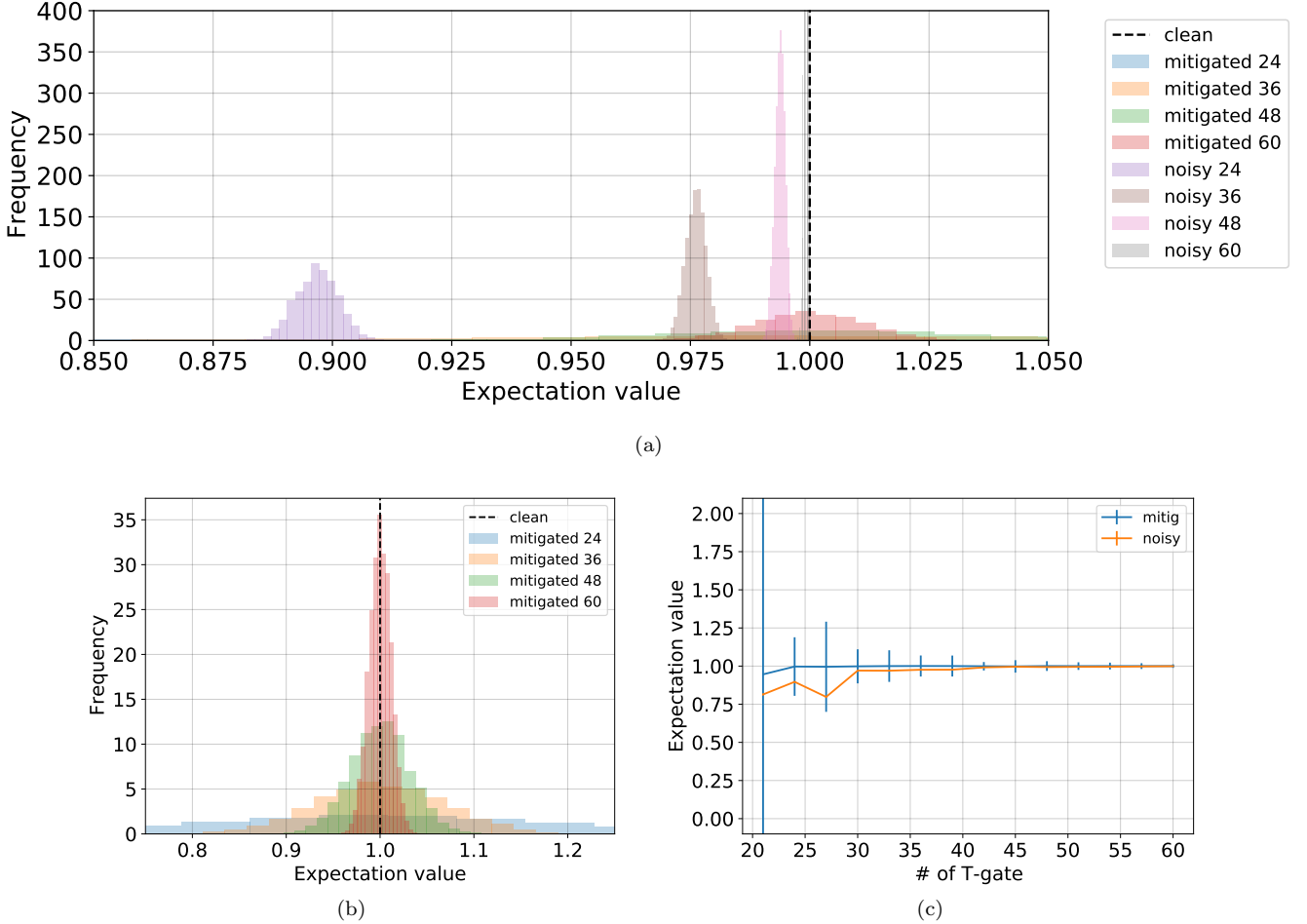


FIG. 7. A histogram for expectation values of SWAP test with approximation errors. (a) A histogram of expectation values. (b) The same figure zoomed around an ideal expectation value. (c) Sample averages and standard deviation as a function of the allowed number of T -gates.

d syndrome values for reliably estimating recovery operations. Since quantum states are in the logical code space only after recovery operations, actual quantum states are not in the logical codes space during FTQC. This makes hard to evaluate logical noise map for several cycles during FTQC because this map does not take a logical state to another logical state, while we need to evaluate logical error map in advance for performing QEM on the code space. To avoid this problem, we employ the following assumption. Suppose that we can perform perfect syndrome measurements in the ld -th cycle where $l = 1, 2, \dots$ and can perform recovery operations just after that, a quantum state is in the logical code space in the ld -th cycle. In this case, we can define a logical error map \mathcal{M}_{dec} from the $(l-1)d$ -th cycle to the ld -th cycle. Here, we assume that if we have a logical operation \mathcal{U} which requires χd cycles, a logical map including effective decoding errors can be approximated with $\mathcal{M}_{\text{dec}}^{\chi} \mathcal{U}$ when code distance d is sufficiently large. If this assumption holds, we can perform QEM for each logical operation for cancelling noise map $\mathcal{M}_{\text{dec}}^{\chi}$. In the main text, although

actual χ depends on logical operations, we assume that $\chi = 1$ for simplicity.

To verify that this assumption holds at least when physical errors are stochastic Pauli noise, we perform the following numerical analysis. Let $\mathcal{M}_{\text{dec},c}$ be a noise map for c -cycle idling of a single logical qubit with code distance d , and let $\Lambda^{(c)}$ be a Pauli transfer matrix of $\mathcal{M}_{\text{dec},c}$. Here, $\mathcal{M}_{\text{dec},c}$ is a stochastic noise map since stochastic Pauli error can only cause logical Pauli errors, and thus $\Lambda^{(c)}$ is a diagonal matrix. Our assumption can be rephrased as follows: There is an effective Pauli transfer matrix Λ_{eff} such that $\Lambda^{(c)} = \Lambda_{\text{eff}}^c$ for sufficiently large c . Equivalently, we assume that each diagonal elements decays exponentially to the number of cycles c . Since Λ_{00} is always unity for stochastic Pauli errors, we are interested in the other diagonal elements. Diagonal elements except Λ_{00} are shown according to the number of cycles in Fig. 8. We utilize the same settings as Sec. V A 2, i.e., depolarizing noise map with $p = 0.01$. Note that Λ_{33} and Λ_{11} are equal since the behavior of surface codes is symmetric for Pauli- X and Z errors. Numerical results are

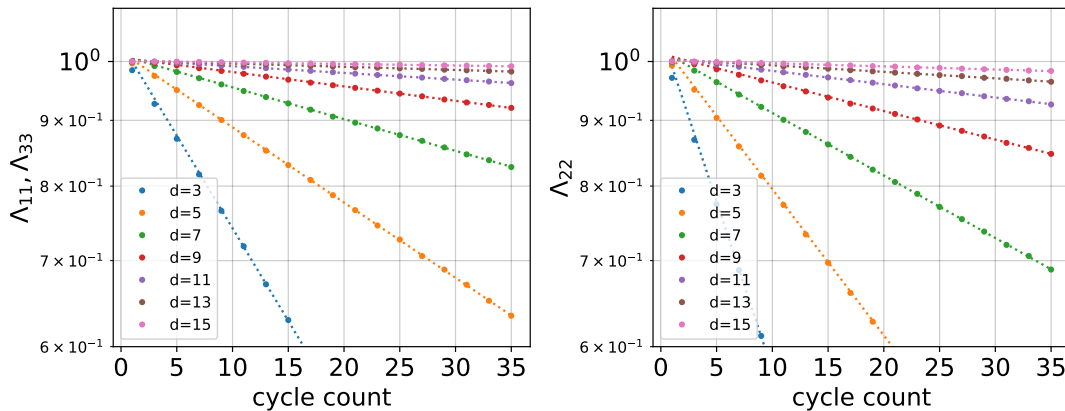


FIG. 8. Diagonal elements of Pauli-transfer matrix for a noise map of a single logical qubit during c syndrome-measurement cycles are plotted according to the code cycles. Each color corresponds to the code distance of a logical qubit. Numerical results are plotted with circle markers, and broken lines are fitting results with exponentially decaying function.

plotted with circle markers, and broken lines are fitting results with exponentially decaying function. We used data points with $c > 20$ for fitting. Their behavior agree well with our assumption except the region where cycle count c is around 1. Thus, we can conclude that if a physical error is stochastic Pauli noise, we can define an effective logical noise map for each logical operation.

Next, we discuss the case when physical noise cannot be modeled as a stochastic Pauli. In practice, the noise of calibrated quantum operations is expected to be stochastic Pauli, since unitary component in physical errors can be canceled by echoing. Nevertheless, there may be non-negligible coherence in quantum noise. In this case, we need to twirl this noise map and remove the unitary component of noise. We show that we can perform twirling on logical noise caused by logical Clifford operations if logical Pauli operations with physical operations, i.e., logical Pauli operations without updating Pauli frame, can be achieved with negligible error rates. Note that logical error rates caused by logical Pauli operations are expected to be sufficiently small compared with those by logical Clifford operations. This is because logical Pauli operations can be performed with transversal single-qubit operations completed in a single cycle, and errors caused by these operations are negligible compared with those by two-qubit operations for stabilizer measurements. Suppose that we perform logical Clifford operation \mathcal{C} and a logical noise map $\mathcal{M}_{\text{dec}}^X$ follows it, and we perform twirling noise $\mathcal{M}_{\text{dec}}^X$ with a set of Pauli operators \mathbb{S} . Then, the twirling process can be described as follows:

$$\left(\frac{1}{|\mathbb{S}|} \sum_{\mathcal{P} \in \mathbb{S}} \mathcal{P} \mathcal{M}_{\text{dec}}^X \mathcal{P} \right) \mathcal{C} = \frac{1}{|\mathbb{S}|} \sum_{\mathcal{P} \in \mathbb{S}} \mathcal{P} \mathcal{M}_{\text{dec}}^X \mathcal{C} (\mathcal{C}^\dagger \mathcal{P} \mathcal{C}), \quad (\text{A1})$$

where \mathcal{P} is a superoperator of logical Pauli operations. Since $\mathcal{C}^\dagger \mathcal{P} \mathcal{C}$ is a logical Pauli operation, twirling of $\mathcal{M}_{\text{dec}}^X$ can be done only with logical Pauli operations. We can

make the same arguments for Pauli measurements and feedback operations dependent on their outcomes. Since all the elemental logical operations except for magic state injection are Clifford operations or Pauli channels, we can apply Pauli twirling to most of the quantum operations in FTQC. Note that while logical Pauli operations for computation can be done by updating a Pauli frame, logical Pauli operations for twirling requires physical implementation on quantum devices. This is because logical Pauli operations by updating a Pauli frame must be tracked after every successive logical operation that we take into account. For example, when we consider general noise $\mathcal{M}_{\text{dec}}^X$, which is not necessarily stochastic Pauli noise, an operator $P' = \mathcal{M}_{\text{dec}}^X \mathcal{P} \mathcal{M}_{\text{dec}}^X$ is not a Pauli operator in general, and thus we cannot continue tracking a frame as a Pauli operator. Thus Pauli twirling must be done physically.

Appendix B: Surface code and lattice surgery

While an applicable scope of our proposal is not limited to a specific architecture of FTQC, we consider FTQC with surface codes and lattice surgery as an example. Surface code [18, 19] is considered as one of the most promising quantum error-correcting codes for integrated devices such as superconducting qubits. This is because surface code has a large threshold value, and its stabilizer measurements can be done in a short and constant depth, and it requires physical qubits that are allocated in a two-dimensional grid and interact only with the nearest neighboring ones. An array of logical qubits is shown in Fig. 9. There are 9 deeply colored patches in the figure, each of which corresponds to a logical qubit. Data qubits are allocated on vertices of deep red and blue faces. Red and blue faces in each patch correspond to stabilizer operators which act on its vertices as Pauli-Z and Pauli-X operators, respectively. The width of a deeply colored

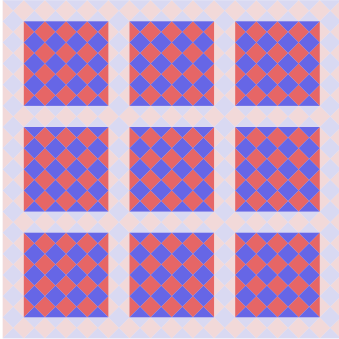


FIG. 9. The schematic of 9 logical qubits for $d = 5$ surface code. Vertices of blue and red squares are corresponding to physical qubits. A bold patch consisting of blue and red faces represents a single logical qubit. In each logical qubit, each bold red and blue face represents Pauli- Z and Pauli- X stabilizer operators acting on its vertices, respectively.

patch d is equivalent to a code distance. Thus, we use $O(d^2)$ physical qubits per logical qubit for surface codes with code distance d . Note that while we can reduce the number of physical qubits by using rotated surface codes [6], we use surface codes shown in Fig. 9 for a simple numerical simulation.

Meanwhile, lattice surgery [6, 7] is a method to increase the number of logical qubits and perform logical two-qubit gates with physical qubits on planer topology. When we prepare logical qubits as patches, we can perform Hadamard gate transversally. Although a logical CNOT-gate is also transversal in surface codes, we cannot perform it fault-tolerantly in planer topology. Instead, we implement multi-qubit Pauli measurements by merging and splitting patches corresponding to logical qubits. By using multi-qubit Pauli measurements and feed-forward operations, we can indirectly perform logical two-qubit Clifford gates fault-tolerantly. For non-transversal operations, we need to inject and distill two types of magic states $|A\rangle$ and $|Y\rangle = SH|0\rangle$ where $S = \exp(i\frac{\pi}{4}Z)$. Unlike magic state $|A\rangle$, since we can perform S -gate using $|Y\rangle$ without consuming a magic state, the number of required $|A\rangle$ is dominant in computation.

Although we choose a strategy of FTQC mentioned above in the main text, there are several other possible strategies for the choice of codes and logical operations to improve efficiency and feasibility. We can also construct logical qubits as defect-pairs in a single large patch and perform a two-qubit Clifford gates with braiding [5]. We can also use concatenated Steane codes or color codes if we can perform CNOT operations more flexibly. S -gate can be achieved with code deformation [45] instead of magic state injection and distillation. We can choose

CCZ -gate as a magic state instead of T -gate [46]. We can estimate recovery operations with algorithms which achieve small latency with threshold degradation [31, 47]. In any case, our method is general; therefore we expect our proposal can be applied naturally.

Appendix C: Coefficients for quasi-probability decomposition

According to Ref. [10], any CPTP-map can be represented as a linear combination of Clifford operations and Pauli channels. We introduce the following 16 operators:

$$\mathcal{B} = \left\{ I, \sigma_j, \frac{I + i\sigma_j}{\sqrt{2}}, \frac{I + \sigma_j}{2}, \frac{\sigma_j + \sigma_{j+1}}{\sqrt{2}}, \frac{\sigma_j + i\sigma_{j+1}}{2} \right\}, \quad (\text{C1})$$

where $j \in \{1, 2, 3\}$, $(\sigma_1, \sigma_2, \sigma_3) = (X, Y, Z)$ and $\sigma_4 = \sigma_1$. The Pauli transfer matrices of $\mathcal{B}^{\otimes m}$ comprise a complete basis of $4^m \times 4^m$ real matrix. Thus, any map can be represented as a linear combination of them. Due to this property, in FTQC, we can perform error cancellation of any noise without non-Clifford gates.

Specifically, when noise is modelled as stochastic Pauli errors, we can cancel it only with Pauli operations. This is because the Pauli transfer matrix of a stochastic Pauli map is diagonal, and any diagonal Pauli transfer matrix can be decomposed only with m -qubit Pauli operations. In FTQC, this means we can cancel stochastic logical Pauli noise only by updating Pauli frame. Suppose that the noise model is described by a superoperator acting on m qubits:

$$\mathcal{N}_{\text{Pauli}} = (1 - p_{\text{err}})\mathcal{I} + \sum_{g \neq I^{\otimes m}} p_g \mathcal{P}_g, \quad (\text{C2})$$

where \mathcal{I} is an identity map, \mathcal{P}_g is a superoperator for Pauli operator g , p_g ($g \in \{I, X, Y, Z\}^{\otimes m}$) is a probability where Pauli error g occurs, and $p_{\text{err}} = \sum_{g \neq I^{\otimes m}} p_g$. This noise can be canceled with the following map:

$$\mathcal{N}_{\text{Pauli}}^{-1} = \sum_g \eta_g \mathcal{P}_g, \quad (\text{C3})$$

where

$$\eta_g = 4^{-n} \sum_{g'} \frac{c(g, g')}{\sum_{g''} p_{g''} c(g', g'')}. \quad (\text{C4})$$

Note that $c(g, g')$ is a function for two Pauli operators such that $c(g, g') = 1$ if $gg' = g'g$ and $c(g, g') = -1$ otherwise. In the case of a single-qubit Pauli noise, coefficients and QEM cost γ_Q can be explicitly given as follows.

$$\begin{aligned}
\eta_I &= \frac{1}{4} \left(1 + \frac{1}{1-2(p_Y+p_Z)} + \frac{1}{1-2(p_Z+p_X)} + \frac{1}{1-2(p_X+p_Y)} \right) \\
\eta_X &= \frac{1}{4} \left(1 + \frac{1}{1-2(p_Y+p_Z)} - \frac{1}{1-2(p_Z+p_X)} - \frac{1}{1-2(p_X+p_Y)} \right) \\
\eta_Y &= \frac{1}{4} \left(1 - \frac{1}{1-2(p_Y+p_Z)} + \frac{1}{1-2(p_Z+p_X)} - \frac{1}{1-2(p_X+p_Y)} \right) \\
\eta_Z &= \frac{1}{4} \left(1 - \frac{1}{1-2(p_Y+p_Z)} - \frac{1}{1-2(p_Z+p_X)} + \frac{1}{1-2(p_X+p_Y)} \right) \\
\gamma_Q &= \sum_{g \in \{I, X, Y, Z\}} |\eta_g| = \frac{1}{2} \left(-1 + \frac{1}{1-2(p_Y+p_Z)} + \frac{1}{1-2(p_Z+p_X)} + \frac{1}{1-2(p_X+p_Y)} \right)
\end{aligned} \tag{C5}$$

Next, we show that the first order approximation of a QEM cost for stochastic Pauli noise is Eq. (12). Consider an unphysical map as follows:

$$\mathcal{N}'_{\text{Pauli}} \equiv (1 + p_{\text{err}})\mathcal{I} - \sum_{g \neq I^{\otimes m}} p_g \mathcal{P}_g, \tag{C6}$$

and we can easily show

$$\|\mathcal{N}'_{\text{Pauli}} \mathcal{N}_{\text{Pauli}} - \mathcal{I}\| \leq 4p_{\text{err}}^2, \tag{C7}$$

where $\|\cdot\|$ denotes an operator norm for Pauli transfer matrix representation of a given superoperator. Then we can see that $\mathcal{N}_{\text{Pauli}}$ is the approximation of the inverse map $\mathcal{N}'_{\text{Pauli}}^{-1}$ up to the first order, and we have $\mathcal{N}'_{\text{Pauli}} = \mathcal{N}_{\text{Pauli}}^{-1} + O(p_{\text{err}}^2)$. Then the QEM cost is approximated as

$$\gamma_Q \approx p_{\text{err}} + \sum_g p_g = 1 + 2p_{\text{err}} \tag{C8}$$

when $p_{\text{err}} \ll 1$.

Appendix D: Details of numerical analysis

In this Appendix, we describe details of numerical simulations in this paper. First, we describe numerical simulations for evaluating decoding errors. In the simulation, we adopt a uniform depolarizing noise model, which occurs on each physical qubit independently and acts as follows:

$$\mathcal{E}(\rho) = (1-p)\rho + \frac{p}{3}(X\rho X + Y\rho Y + Z\rho Z). \tag{D1}$$

This error acts on data qubits at the beginning of each cycle and acts on ancillary qubits just before its measurement. As shown in the main text, we assume perfect syndrome measurements at the 0-th and d -th cycles, which guarantees that quantum states at these cycles are in logical space with recovery operations regardless of whether decoding is successful or not. Then, we evaluate logical error probabilities during these cycles. For estimating a recovery operation of logical operations, we used

minimum-weight perfect matching decoder [18]. This decoder reduces the problem of decoding to an instance of a minimum-weight perfect matching problem. While this problem is NP-hard when there are Pauli- Y errors, we can approximately solve this problem by using Edmonds' blossom algorithm [32]. It is known that surface codes show threshold behavior even with this approximation. We use an implementation in Ref [48] for solving this problem. To estimate the logical error rate, we evaluate 10^5 samples for each data point in Fig. 3(b) and 10^6 samples for the other figures.

In the performance evaluation of error mitigation for decoding errors, we assume an error channel for each logical gate is a non-uniform logical depolarizing channel obtained in the benchmark of logical error probabilities in surface codes. Since there is no perfect syndrome measurement in practice, this assumption does not hold exactly. Nevertheless, this approximation is asymptotically correct, and thus we employed this assumption to evaluate the performance of QEM for logical errors.

For the simulation of Clifford circuits, we used a stabilizer circuit simulator of which the memory allocations are optimized so that update for actions of Clifford operations becomes sequential. With this technique, simulation of stabilizer circuits dominated by Clifford operations rather than Pauli measurements becomes hundreds of times faster than the existing implementation stabilizer simulators [33].

For Solovay-Kitaev algorithm, we use a method and implementation proposed and published in Ref. [29]. While we need to limit the allowed number of T -gates, this method outputs a sequence of Clifford and T gates according to an allowed error rate ε . Thus, we searched the minimum error rate ε^* with which the algorithm outputs a sequence with the number of T -gates smaller than the allowed number of T -gates. This search is done with a simple bisection method and repeated until accuracy reaches 10^{-14} . For the simulation of SWAP test circuits, we use Qulacs [49], which is a simulator for general noisy quantum circuits and is fast especially when we perform a huge number of simulations of small quantum circuits.

-
- [1] P. W. Shor, SIAM review **41**, 303 (1999).
- [2] A. W. Harrow, A. Hassidim, and S. Lloyd, Physical review letters **103**, 150502 (2009).
- [3] M. A. Nielsen and I. Chuang, “Quantum computation and quantum information,” (2002).
- [4] D. A. Lidar and T. A. Brun, *Quantum error correction* (Cambridge University Press, 2013).
- [5] A. G. Fowler, M. Mariantoni, J. M. Martinis, and A. N. Cleland, Physical Review A **86**, 032324 (2012).
- [6] C. Horsman, A. G. Fowler, S. Devitt, and R. Van Meter, New Journal of Physics **14**, 123011 (2012).
- [7] A. G. Fowler and C. Gidney, arXiv preprint arXiv:1808.06709 (2018).
- [8] K. Temme, S. Bravyi, and J. M. Gambetta, Physical review letters **119**, 180509 (2017).
- [9] Y. Li and S. C. Benjamin, Physical Review X **7**, 021050 (2017).
- [10] S. Endo, S. C. Benjamin, and Y. Li, Physical Review X **8**, 031027 (2018).
- [11] J. Sun, X. Yuan, T. Tsunoda, V. Vedral, S. C. Benjamin, and S. Endo, arXiv preprint arXiv:2001.04891 (2020).
- [12] S. McArdle, X. Yuan, and S. Benjamin, Physical review letters **122**, 180501 (2019).
- [13] X. Bonet-Monroig, R. Sagastizabal, M. Singh, and T. O’Brien, Physical Review A **98**, 062339 (2018).
- [14] Z. Cai, arXiv preprint arXiv:2007.01265 (2020).
- [15] A. Strikis, D. Qin, Y. Chen, S. C. Benjamin, and Y. Li, arXiv preprint arXiv:2005.07601 (2020).
- [16] P. Czarnik, A. Arrasmith, P. J. Coles, and L. Cincio, arXiv preprint arXiv:2005.10189 (2020).
- [17] S. Endo, Z. Cai, S. C. Benjamin, and X. Yuan, arXiv preprint arXiv:2011.01382 (2020).
- [18] E. Dennis, A. Kitaev, A. Landahl, and J. Preskill, Journal of Mathematical Physics **43**, 4452 (2002).
- [19] S. B. Bravyi and A. Y. Kitaev, arXiv preprint quant-ph/9811052 (1998).
- [20] A. Y. Kitaev, Russian Mathematical Surveys **52**, 1191 (1997).
- [21] C. M. Dawson and M. A. Nielsen, arXiv preprint quant-ph/0505030 (2005).
- [22] R. Blume-Kohout, J. K. Gamble, E. Nielsen, J. Mizrahi, J. D. Sterk, and P. Maunz, arXiv preprint arXiv:1310.4492 (2013).
- [23] D. Greenbaum, arXiv preprint arXiv:1509.02921 (2015).
- [24] D. Gottesman, arXiv preprint quant-ph/9705052 (1997).
- [25] B. Eastin and E. Knill, Physical review letters **102**, 110502 (2009).
- [26] L. Rieseboos, X. Fu, S. Varsamopoulos, C. G. Almudever, and K. Bertels, in *Proceedings of the 54th Annual Design Automation Conference 2017* (2017) pp. 1–6.
- [27] N. C. Jones, R. Van Meter, A. G. Fowler, P. L. McMahon, J. Kim, T. D. Ladd, and Y. Yamamoto, Physical Review X **2**, 031007 (2012).
- [28] A. G. Fowler, A. C. Whiteside, and L. C. Hollenberg, Physical review letters **108**, 180501 (2012).
- [29] N. J. Ross and P. Selinger, arXiv preprint arXiv:1403.2975 (2014).
- [30] C. Wang, J. Harrington, and J. Preskill, Annals of Physics **303**, 31 (2003).
- [31] N. Delfosse and N. H. Nickerson, arXiv preprint arXiv:1709.06218 (2017).
- [32] J. Edmonds, Canadian Journal of mathematics **17**, 449 (1965).
- [33] S. Aaronson and D. Gottesman, Physical Review A **70**, 052328 (2004).
- [34] A. K. Ekert, C. M. Alves, D. K. Oi, M. Horodecki, P. Horodecki, and L. C. Kwek, Physical review letters **88**, 217901 (2002).
- [35] S. Lloyd, Science , 1073 (1996).
- [36] D. W. Berry, A. M. Childs, R. Cleve, R. Kothari, and R. D. Somma, Physical review letters **114**, 090502 (2015).
- [37] G. H. Low and I. L. Chuang, Quantum **3**, 163 (2019).
- [38] G. H. Low and I. L. Chuang, Physical review letters **118**, 010501 (2017).
- [39] S. Endo, Q. Zhao, Y. Li, S. Benjamin, and X. Yuan, Physical Review A **99**, 012334 (2019).
- [40] A. C. Vazquez, R. Hiptmair, and S. Woerner, arXiv preprint arXiv:2009.04484 (2020).
- [41] K. Mitarai and K. Fujii, arXiv preprint arXiv:1909.07534 (2019).
- [42] K. Mitarai and K. Fujii, arXiv preprint arXiv:2006.11174 (2020).
- [43] J. R. McClean, Z. Jiang, N. C. Rubin, R. Babbush, and H. Neven, Nature Communications **11**, 1 (2020).
- [44] J. R. McClean, M. E. Kimchi-Schwartz, J. Carter, and W. A. De Jong, Physical Review A **95**, 042308 (2017).
- [45] B. J. Brown, K. Laubscher, M. S. Kesselring, and J. R. Wootton, Physical Review X **7**, 021029 (2017).
- [46] C. Gidney and A. G. Fowler, Quantum **3**, 135 (2019).
- [47] A. Holmes, M. R. Jokar, G. Pasandi, Y. Ding, M. Pedram, and F. T. Chong, arXiv preprint arXiv:2004.04794 (2020).
- [48] V. Kolmogorov, Mathematical Programming Computation **1**, 43 (2009).
- [49] “Qulacs,” (2018), <https://github.com/qulacs/qulacs>.